Arabian Journal of Chemistry (2021) **14**, 102959

King Saud University

**Arabian Journal of Chemistry**

www.ksu.edu.sa
www.sciencedirect.com

ORIGINAL ARTICLE

# Design of a solar reactor for the removal of uranium from simulated nuclear wastewater with oil-apatite ELM system

**Ali Aghababai Beni**

*Department of Chemical Engineering, Shahrekord Branch, Islamic Azad University, Shahrekord, Iran*

Received 18 October 2020; accepted 16 December 2020
Available online 21 December 2020

**KEYWORDS**

Adsorption;
Uranium(VI);
Solar reactor;
Emulsion liquid membrane;
Nano-Hydroxyapatite

**Abstract** Nuclear wastewater containing uranium ions is a serious threat to the environment. In this study, uranium (VI) ions were adsorbed from the synthesized wastewater by hydroxyapatite nanoparticles (NHAP) in the emulsion liquid membrane (ELM) process. The NHAP was dispersed in the oil, and ELM globules were formed by injecting the NHAP-oil phase into the wastewater. The FT-IR of NHAP, before and after separation process showed the hydroxyl, amine, and phosphoryl groups are important to immobilization of U(VI) ions in oil phase. The morphology of NHAP was identified with FE-SEM, with the NHAP size intially 50 nm, while and at the end the size was about 1 $\mu$m. The following optimum conditions were selected: pH = 4, NHAP concentration = 12.4 $gL^{-1}$, volume of ELM = 43 ml, retention time = 45 min, air flow rate = 0.5 L $min^{-1}$ and impeller rotation speed = 200 rpm. The viscosity of the oil phase decreased with solar radiation and the U(VI) adsorption on the NHAP surface was improved. The oil and air phase distribution within the water phase was simulated. Adsorption isotherms, thermodynamic parameters and kinetic data were investigated.


## 1. Introduction

The development of nuclear power plants, in recent years, has generated large amounts of uranium wastewater (Wu et al., 2019). Nuclear wastewater discharges into the environment create serious risks for human health, animals and plants, even at very low concentrations (Christou et al., 2019). Uranium enters the body causing kidney disease and toxicity to the bones (Shin et al., 2016). According to the law of the World Health Organization (WHO), the maximum contamination level (MCL) of U(VI) ions in drinking water is 30 $\mu g\ L^{-1}$ as the permissible limit of uranium concentration

E-mail address: aliaghababai@yahoo.com
Peer review under responsibility of King Saud University.

Production and hosting by Elsevier

https://doi.org/10.1016/j.arabjc.2020.102959

(Sahu et al., 2020). In addition to the importance of industrial wastewater treatment to protect the environment from the risk of emission of radioactive contaminants, uranium separation for reuse in the nuclear fuel cycle is an important and strategic issue (Jain et al., 2018).

Recently, heavy metals removal by biosorbents was introduced. Reports showed that biologically derived materials such as brown algae (Beni and Esmaeili, 2019b; Esmaeili and Beni, 2015) or chitosan (Esmaeili and Beni, 2014) extracted from shrimp skin had high adsorption capacity. Hydroxyapatite is one of the sorbents that has attracted the attention of researchers today (Holmes et al., 2012; Long et al., 2019). The adsorption capacity of U(VI) ions on hydroxyapatite depends on the phosphate, calcium and oxygen contained in the apatite (Han et al., 2018). The crystallinity morphology of hydroxyapatite with high surface area affects ions adsorption.; whereas, by changing the furnace temperature and the rate of temperature increase, the specific surface of hydroxyapatite can be improved (Googerdchian et al., 2018). In addition, recently hydroxyapatite-based adsorbents can be modified or coupled with other adsorbents. for example Piccirillo et al. (Piccirillo et al., 2013) immobilised gram-negative bacterial strains on the surface of fishbone hydroxyapatite, claiming that this structural technique increased the elimination efficiency of cadmium and zinc ions. Similarly, Sundaram et al. (Sundaram et al., 2009) produced nano-hydroxyapatite/chitin composite for fluoride sorption.

Solvent extraction is the best known method for recycling uranium (Mesli and Belkhouche, 2018). But if the uranium concentration is less than 1 g $L^{-1}$, the mass transfer driving force for extraction is low (Banat et al., 2000; Kulkarni et al., 2018), so this process is not an economical method, because a large solvent is required (Davoodi-Nasab et al., 2018). However, ELM process is a better removal method to replace other separation techniques and much research has been done to improve ELM (Zereshki et al., 2018). ELM has three-phase water/oil/water system which are obtained by the dispersion of water/oil emulsion globules in an wastewater phase (Benderrag et al., 2019). Usually globules are formed by water phase in oil emulsion then dispersed in the other water phase as external phase (Ferreira et al., 2019). ELM has more advantages than solvent extraction, including: the simplicity of the process, less energy consumption, less extractant consumption, and high interface for mass transfer by disperse of globules in the external phase (Kumar et al., 2019b). Fig. 1 presents a diagram for the formation and phase separations of ELM system. Although the ELM separation process is effective, its industrial application is limited (Kohli et al., 2019). because the globules are not stable in large volume mixing conditions. Emulsion stability in ELMs is defined by the resistance of the globules against destruction under high shear stress (Davoodi-Nasab et al., 2017). Destruction means the coalescence and rupture; also the swelling, creaming and flocculation influence on the rupture of globules (Kohli et al., 2019). By adding a surfactant to a ELM system even at low concentration, the surface tension decreases and the average size of the globules decreases, therefore the coalescence decreases and the stability the emulsion improves (Davoodi-Nasab et al., 2019; Zereshki et al., 2018). But surfactants are toxic and environmental pollutants (El Haddad et al., 2013). Recently, researchers used of nanomaterials in the ELM structure. The use nanoparticles and surfactants prevents creaming and coalescing (Kohli et al., 2019) also, this structure reduces the amount of surfactant (Davoodi-Nasab et al., 2017). Although in previous work, despite the use of green surfactants and nano-materials, the emulsion stability problem was not resolved definitively (Ahmad et al., 2011). Table 1 compares the methods of removing heavy metal ions from industrial wastewater.

In this paper, for the first time, the presence of hydroxyapatite nanoparticles in the internal aqueous phase was investigated. One of the advantages of this study was that the

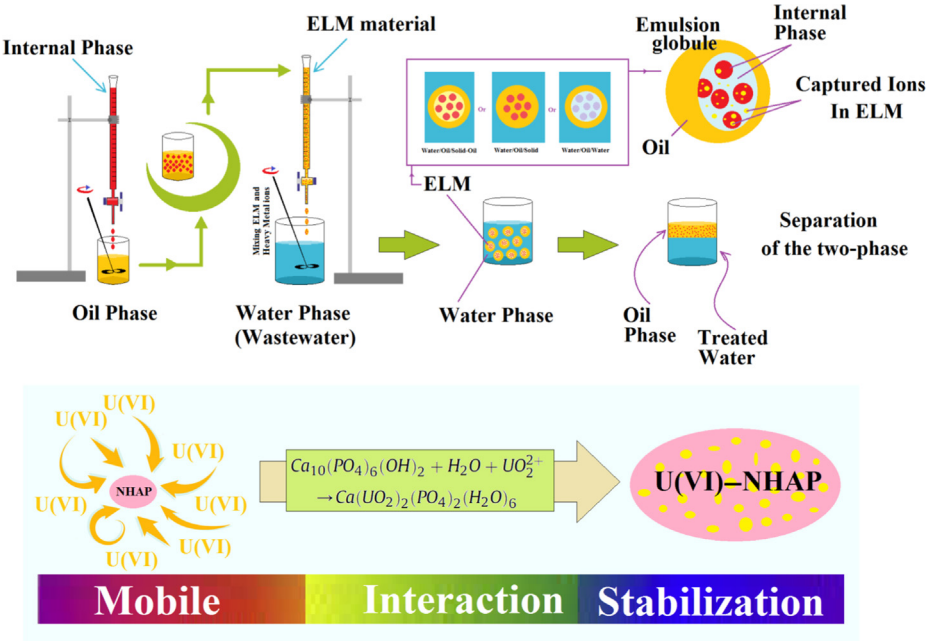


**Fig. 1** Diagram of ELM formation and phase separations and scheme to illustrate the adsorption mechanism.

emulsion system was operated without adding surfactant and the stability of the system was ensured based on the optimization of air intake and mixing rate. The effect of mixing with air injection was tested to increase the removal efficiency of U(VI); also, the effect of solar heating on reducing the viscosity of the oil phase and reducing the mass transfer resistance was investigated. This system is useful for areas that are exposed to sunlight, because in these areas, the system benefits from a free energy source to reduce the viscosity of the emulsion phase.

## 2. Experimental

### 2.1. Material

Bovine bones were purchased from a butcher shop in Shahrekord, Iran. Soybean oil (analytical standard) was obtained from Sigma-Aldrich. Sodium hydroxide (NaOH), hydrochloric acid (HCl) and uranyl nitrate hexahydrate ($UO_2(NO_3)_2.6H_2O$) were preparade from Merck.

### 2.2. Synthesis of NHAP

Bovine bones were crushed to 5 mm of diameter using a hammer. The bones were put into water vapor (steam) at 110 °C for 12 h to remove all fat and tissues, then dried for 24 h at 100 °C in the oven. The bones were placed oven for 6 h at 850 °C in the muffle furnace. The calcined bones were crushed with a planetary ball mill for 2 h at 600 rpm.

### 2.3. Design of process and methodology

According to Fig. 2a the solar reactor was made of cylindrical glass with an inner diameter (105 mm), a length (105 mm) and a thickness (4 mm). The glass cylinder was mounted horizontally with two Plexi retainers. A Flat-blade Turbine impeller was installed in the center of the solar reactor (Details in Fig. S1).

U(VI) effluent was introduced into the solar reactor in a volume of 600 ml. To test the NHAP concentration, the NHAP was added to the soybean oil at a concentration of 0.25–20 g $L^{-1}$ at 28 °C for 2 h at 1500 rpm stirring. The oil-NHAP nano-fluid was loaded in three syringes (5-ml) and syringes were placed on a syringe pump; a vibrator was mounted to the syringe to prevent the nanoparticles deposition. The discharge rate of the oil phase within the solar reactor was 10 ml $min^{-1}$ from each syringe. To test the ELM volume, the volume of 10–60 ml of emulsion section was added to the feed phase in the solar reactor. The solar reactor equipped with an air pump. The ELM globules contacted with U(VI) effluent under stirring and aeration condition. Solar heat energy was used to investigate the effect of temperature on the reduction of oil phase viscosity; this innovative technique has not been reported in similar cases of ELM systems. The solar simulator (NanoSAT-IIIS-200, Iran) with an AM 1.5 filter and light intensity of 1 kW $m^{-2}$ was used to simulate solar light. The unit temperature was measured and recorded using a laser thermometer (Etekcity Lasergrip 774 Non-contact Digital Laser Infrared Thermometer). The temperature at zero time was 25 °C ± 0.5 °C. The effect of temperature was tested from 28 to 45 °C. U(VI) ions passed through the oil phase and stabilized on NHAP active sites within the emulsion phase nucleus. Oil phase was separated from the aqueous phase after completion of the process, the impeller was turned off and the system was biphasic. U(VI) ions were adsorbed by NHAP, a non-woven fabric was used to separate the NHAP from the oil phase. The experiments were performed using Design-Expert 11 with RSM and the CCD. According to Table 2, 5 independent factors were considered including: U(VI) concentration (mg $L^{-1}$), NHAP concentration (g $L^{-1}$), pH, volume of oil-NHAP (ml) and retention time (min), as well as the removal efficiency of U(VI) ions from the synthesized effluent was selected as the response surface. In this case, the Design-Expert software provided the 50 runs with 8 central points; Table S1 presents the pattern of experiments with actual and predicted results. In current study the factor of solar energy, the fluid temperature, the removal efficiency and separation quality were measured in each run. Numerical optimization was performed in the software with the approach of changing the independent factors in lower and upper ranges and the goal of reaching to maximum for the removal efficiency. Statistical analysis of data was performed using MATLAB R2015b.

### 2.4. Characterization and measurement

NHAP functional groups were identified with FT-IR spectra in the 450–4000 $cm^{-1}$ (using a C88731 spectrophotometer, Perkin Elmer Co., Germany). The NHAP morphology was obtained after drying at 40 °C for 2 h and gold coating by field emission SEM (TE-SCAN, Czech). The U(VI) concentration in the sample solution was calculated by ICP-AES (Thermo Jarrell Ash, Model Trace Scan, Canada); All experiments were performed at 25 °C ± 0.5 °C.

### 2.5. CFD simulation

The effect of aeration and impeller rotational speed on the ELM performance were investigated by injecting air at different flow rate (0.2–1.2 L $min^{-1}$) with a syringe needle as a diffuser and 50–500 rpm as different axial velocity of impeller. CFD was investigate the oil phase distribution in water phase by ANSYS fluent 2019R2 at optimum conditions. The geometry of the solar reactor according to Fig. S1 was designed using Gambit 2.4., in the three-phase system, the liquid water was selected as the primary phase, the oil and air as the secondary phases at the Eulerian multiphase model. The standard k-epsilon was selected for viscous model. In all simulations, the SIMPLE algorithm was used, to solve both pressure and velocity in discrete equations. The first order upwind was used to momentum, turbulent kinetic energy, volume fraction and turbulent dissipation rate. Three-phase mixing was analyzed using the MRF approach, taking into account the linear velocity of inlet air and oil, as well as the rotational speed.

## 3. Results and discussion

### 3.1. Investigation of spectroscopy in NHAP

The FT-IR spectrums were used to identify NHAP functional groups before making the ELM and after U(VI) removal process in the ELM system. The hydroxyl, carboxyl, amine, and

**Table 1** Comparison of heavy metal ion removal methods in other studies.

| Reference | Method | Ions | Description |
|---|---|---|---|
| (Han et al., 2018) | Adsorbent: Bio-hydroxyapatite from waste fish bone | U(VI) | High absorption capacity 384.6 mg $g^{-1}$. Absorbent synthesis of waste materials. No separation technique applicable in industry (Batch sorption in Erlenmeyer flasks). High energy consumption. Separation of nanoparticles from fluid is difficult. |
| (Zhao et al., 2014) | Adsorbent: 3-D nanosheet-assembled hydroxyapatite using hemoglobin protein. | Pb(II) | Synthesis as a soft template. Selectively adsorb Pb (II) from solution containing Cd(II), Cu(II) and Pb (II). Separation of adsorbent with high energy centrifuge. Hard operation. Unusable for industry purposes. |
| (Guo et al., 2019) | Adsorbent: Synthesis of bitter gourd-shaped nanoscaled hydroxyapatite | Cd(II); Cr(III) and Pb (II) | Eco-friendly adsorption material. The nano-hydroxyapatite morphology was controlled by adding mono-dodecyl phosphate potassium. No separation technique applicable in industry (Batch sorption in plastic tube). Absorbent synthesis is costly. |
| (Bayramoglu and Yakup Arica, 2019) | Adsorbent: Star type polymer grafted and polyamidoxime modified silica coated-magnetic particles | U(VI) | Synthesis of new adsorbents. High absorption capacity 760.3 mg $g^{-1}$. Good reusability for ten cycles of adsorption–desorption. High stability. Absorbent synthesis is difficult. |
| (Bayramoglu and Yakup Arica, 2016) | Adsorbent: MCM-41 silica particles grafted with polyacrylonitrile | U(VI) | Adsorption on the pristine MCM-41, amidoxime and carboxyl groups. High absorption capacity 58.9, 296.7 and 442.3mg$g^{-1}$. Particles are stable, and easily regenerated. No separation technique applicable in industry. |
| (Yakup Arica et al., 2016) | Adsorbent: Polyaniline coated magnetic carboxymethylcellulose beads | U(VI) | High adsorption capacities 129.4 and 386.5 mg $g^{-1}$ for magnetic carboxymethylcellulose beads and their coated with poly-aniline. Suitable technique for industrial use. |
| (Noah et al., 2020) | ELM: palm oil as diluent, Span 80 as surfactant, trioctylmethylammonium chloride as extractant, and acidic thiourea solution as an internal reagent. | Cr(VI) to Cr (III) | Continuous extractor for chromium recovery; Recovery and enrichment of the less toxic Chromium (III). 99% of Chromium could be extracted at the optimum process conditions, the optimized values of emulsion to an external feed phase ratio, agitation speed and retention time are found to be 1:5, 342 rpm and 170 s. Use of surfactant for system stability. |
| (Ferreira et al., 2019) | ELM: Di-(2-ethylhexyl phosphoric acid), kerosene, NaOH, H2SO4, EDTA and biosurfactant solution from Pseudomonas aeruginosa ATCC 10,145 | Mn(II) | Use of biosurfactants. Fast, economical and efficient process. Low ELM stability (stability time 2 min). Without providing techniques for use in industry. |
| (Parbat et al., 2020) | ELM: kerosene (diluent), span 80 (emulsifier) and NaOH as a stripping agent in the internal phase. | Co(II) | Preparation of ELM using Aliquat 336 carrier. Use of hydrodynamic cavitation. Higher interfacial mass transfer area due to reduced droplet size of emulsion prepared by hydrodynamic cavitation. Speedy transport of heavy metals due to higher interfacial mass transfer area. |
| In this work | ELM: Soybean oil and hydroxyapatite nanoparticles | U(VI) | High stability of the ELM system. Injection of air into the reactor. ELM system without surfactants. Easy separation of nanomaterials from effluents. Use free solar energy. Provide methods and techniques for industrial use near the equator. Stabilization of uranium ions in hydroxyapatite nanoparticles adsorbent. Green and environmentally friendly method. |

phosphoryl groups play important roles in the fixation of U (VI) ions. According to Fig. 2b, —OH groups were observed in the single sorption band at 3570 $cm^{-1}$ and triple bands at 570, 602 and 632 $cm^{-1}$ (Han et al., 2018). The phosphor element, with complex non-bonded electron form, can strong bonds with most materials; the dual band at 1042 and 1092 $cm^{-1}$ with a strong transmission represents (Zhao et al., 2014). The plane bending at 1459 $cm^{-1}$ related to N—H groups

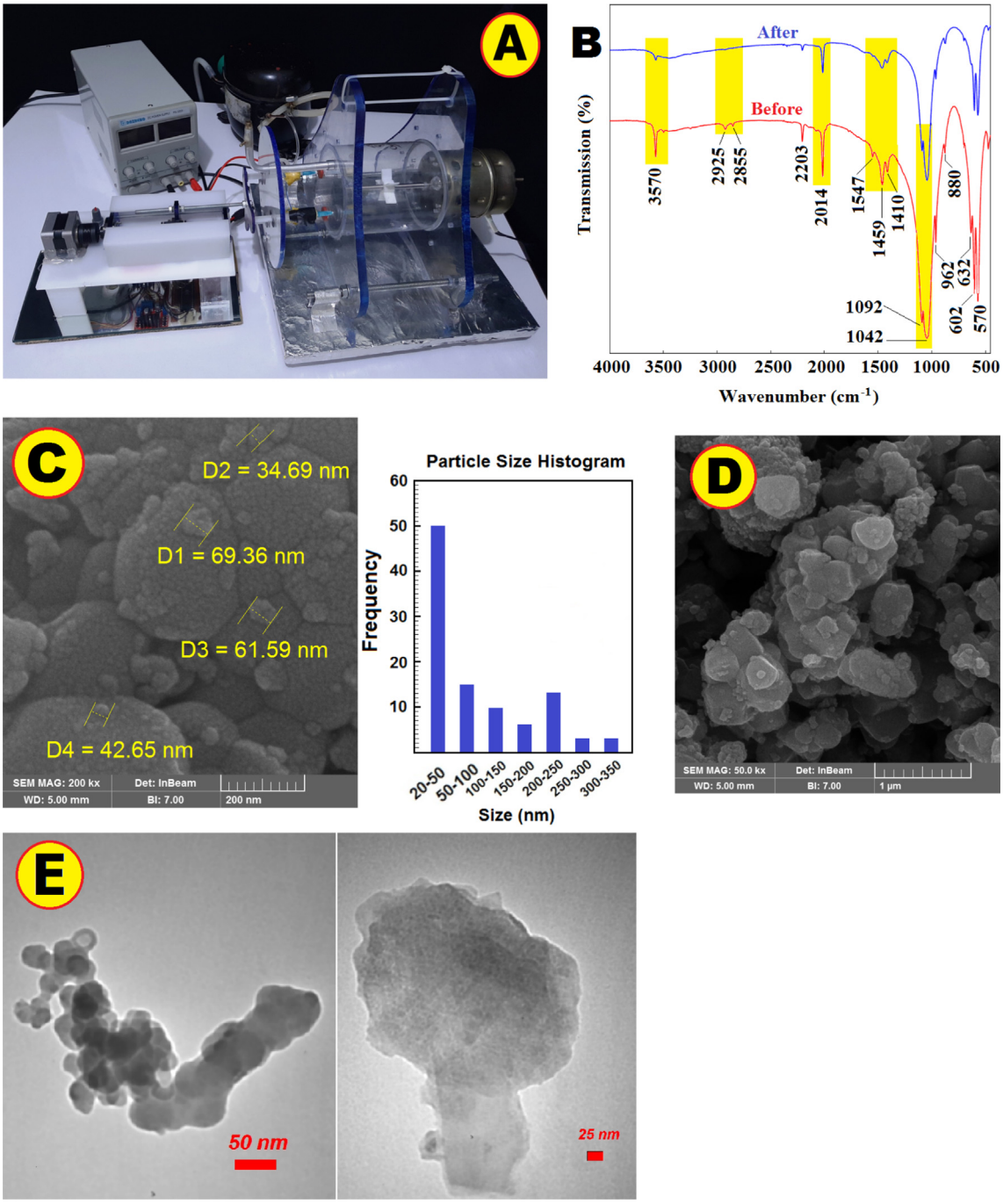


**Fig. 2** Image of real devices used in experiments (A). FT-IR spectra of NHAP before and after U(VI) ions adsorption in the ELM (B). FE-SEM of NHAP before (C) and after U(VI) ions adsorption (D). TEM analysis on NHAP-Uranium (E).

(El Haddad et al., 2013). The lowest intensity peak at 3570 $cm^{-1}$ was attributed to the O—H (Hubadillah et al., 2020). Comparison of the FT-IR spectra showed that U(VI) formed stable ligands with functional groups.

Fig. 2c shown the FE-SEM morphology and microstructure of NHAP. The NHAP before adsorption are visible about less than 50 nm of diameter, also the nanoparticles are attached to each other and formation a propose surface. In Fig. 2d, NHAP are visible after U(VI) ions adsorption, NHAP structure after sorption and removal from the oil and water phase indicates that particles formed clusters less than 1$\mu$m in diameter. TEM analysis was undertaken on NHAP-Uranium (Fig. 2e), and it be visualized as dense bodies.

### *3.2. The effect of aeration, impeller rotational speed and CFD simulation*

At constant values of the affecting variables on the durability of emulsion globules, the effect of impeller rotational speed and air flow rate were tested. The stability index of the globules

**Table 2** Parameter with different values.

| Parameter | Levels | | | | |
|---|---|---|---|---|---|
| | $-\alpha$ | $-1$ | 0 | $+1$ | $+\alpha$ |
| U(VI) concentration (mg $L^{-1}$), $X_1$ | 20 | 140 | 260 | 380 | 500 |
| NHAP concentration (g $L^{-1}$), $X_2$ | 0.25 | 5.19 | 10.1 | 15.1 | 20 |
| pH, $X_3$ | 12 | 9.75 | 7.5 | 5.25 | 3 |
| Volume of ELM (ml), $X_4$ | 10 | 22.5 | 35 | 47.5 | 60 |
| Retention time (min), $X_5$ | 5 | 18.8 | 32.5 | 46.3 | 60 |

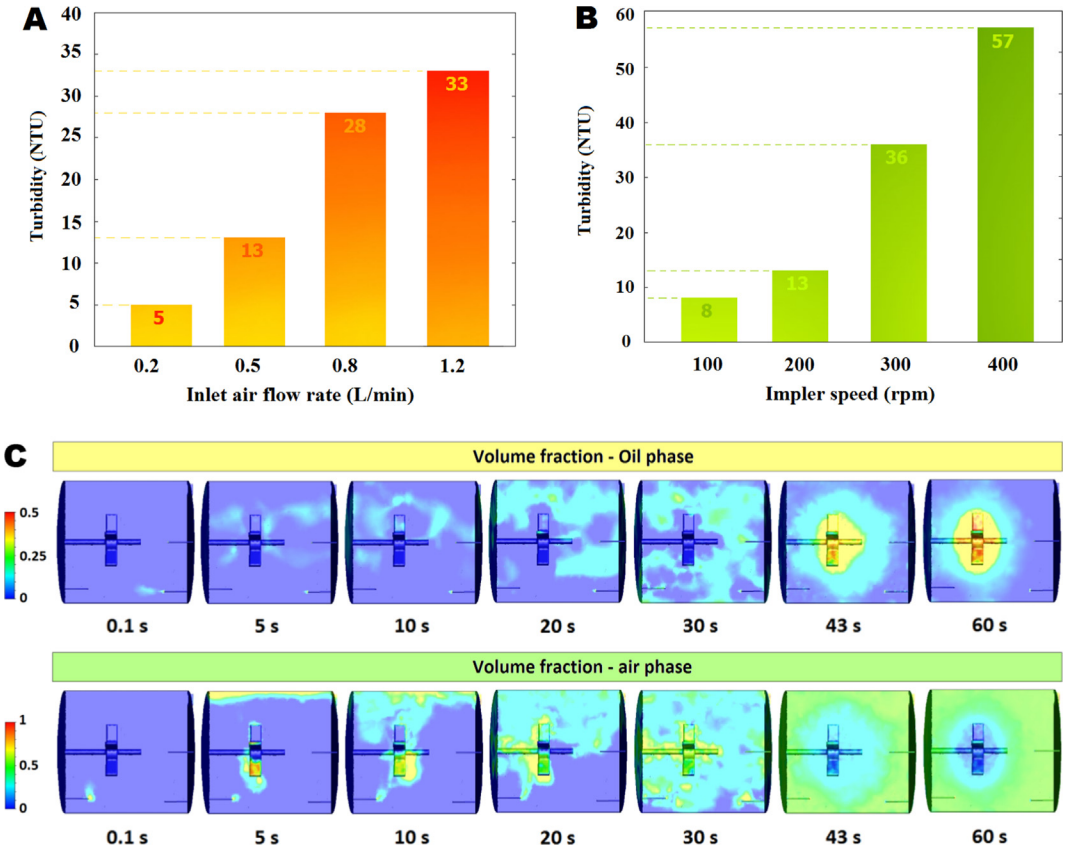


**Fig. 3** Effect of aeration on the durability of emulsion globules with turbidity measurement as stability index @NHAP = 12 $gL^{-1}$, pH = 4, ELM = 43 ml, retention time = 45 min and rotation = 200 rpm (A). Effect of impeller rotational speed on the durability of emulsion globules with turbidity measurement as stability index @NHAP = 12 $gL^{-1}$, pH = 4, ELM = 43 ml, retention time = 45 min and aeration = 0.5 L $min^{-1}$ (B), Oil phase and air phase distribution in water phase under optimum conditions @rotation = 200 rpm and aeration = 0.5 L $min^{-1}$ (C).

was compared with the turbidity (Fig. 3a-b). Increased air flow rate and impeller rotational speed caused rupture of globules, some of the NHAP was removed from the oil phase, and tiny droplets of oil were formed. At low air flow rate (0.2 L $min^{-1}$) and low impeller rotational speed (100 rpm) was observed globules grow by binding to each other and mixing is disrupted. According to this result optimum conditions (0.5 L $min^{-1}$ and 200 rpm) were selected for CFD simulation. Fig. 3c shown distribution of oil and air volume fraction in solar reactor after 0.1–50 s.

### *3.3. Optimization of effective factors in the ELM process*

#### *3.3.1. NHAP concentration in oil phase*

The internal phase in ELM is often an aqueous phase that is present in the oil coating. In this study internal phase was composed of NHAP in the soybean oil. The NHAP concentration in oil was prepared from 0.25 to 20 g $L^{-1}$ and then it was injected into the solar reactor for U(VI) sorption.

According to Fig. 4a with the increase of NHAP concentrations to approximately 12 g $L^{-1}$, removal efficiency increased

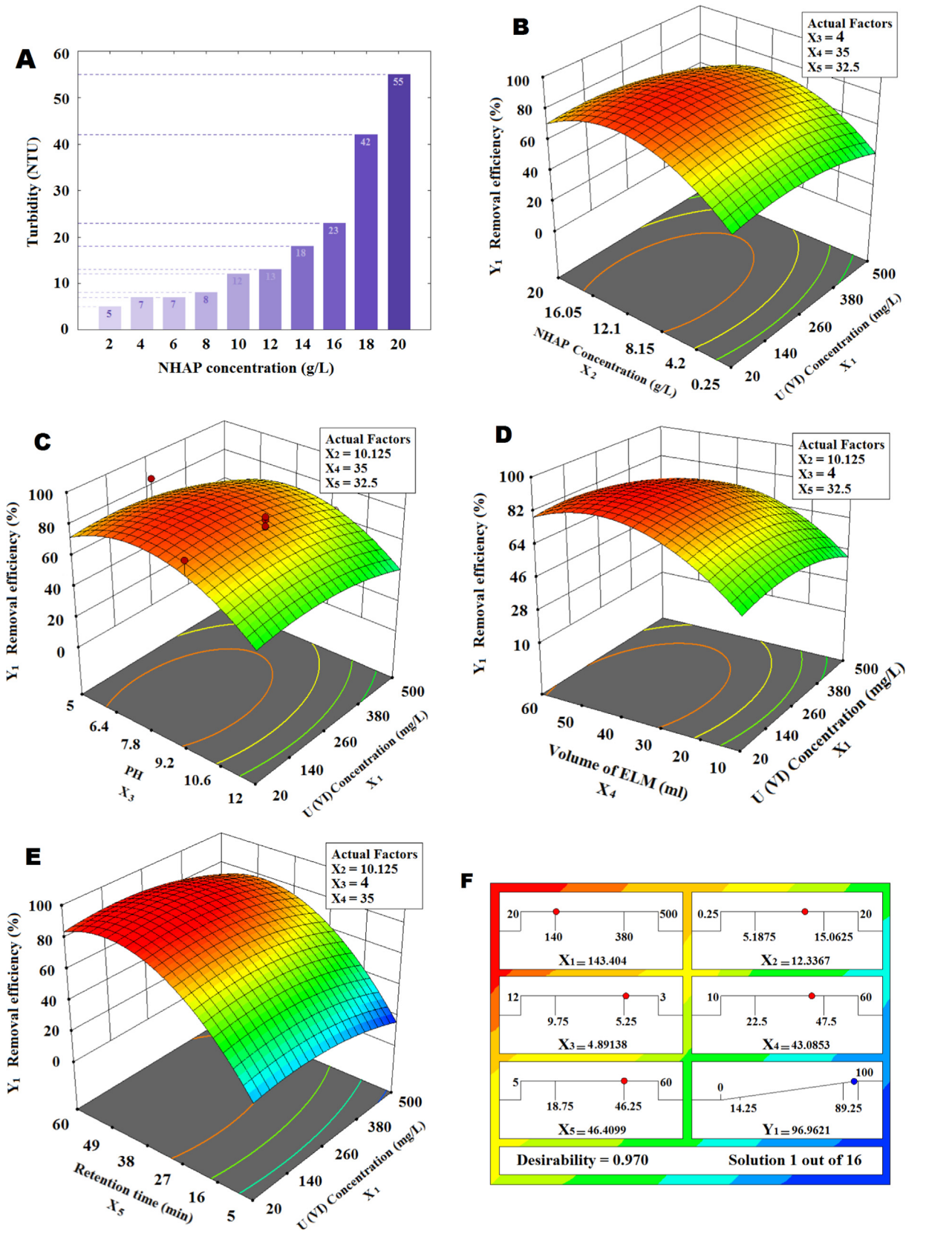


**Fig. 4** Effect of NHAP concentration in emulsion globules on fluid turbidity in the solar reactor (A). Effect of NHAP concentration in oil phase (B), pH (C), volume of ELM (D) and retention time (E) on the U(VI) ions removal efficiency. Ramp (F).

but in greater concentrations of NHAP, the removal efficiency decreased because NHAP was removed from globules and entered the wastewater. Similar to our work, Davoodi-Nasab et al. (2017) and Kohli et al. (2019) used of carbon nanotubes as internal phase in emulsion nano-fluid membrane, they reported: adding more than the optimal amount of adsorbent does not increase the adsorption of contaminants.

Fig. 4b had shown the effect of NHAP concentration on the fluid turbidity at end of ELM process, after stationary time of 45 min, the fluid turbidity in the solar reactor was increased. Increasing internal phase concentration leads to instability, increased swelling and breakage the emulsion globules (Davoodi-Nasab et al., 2019). So, the optimum condition for NHAP concentration was about 12 g $L^{-1}$.

### 3.3.2. The effect of pH in the solar reactor

In the ELM process, the pH is an important parameter to stability and hydrophilicity of the emulsion globule surface. Also, the dissolution of ions in the oil phase depends on the external feed phase pH (Kumar et al., 2019a). NHAP (1 g) in $H_2O$ (25 ml) was dissolved, pH was 11 and NHAP in oil showed that the pH is 10, so NHAP is alkaline due to the presence of $OH^-$. The nature pH of ELM and wastewater solution in solar reactor was 9 and solution pH adjusted by NaOH and HCl. The pH was adjusted at the beginning of each experiment and remained constant until the end of the experiment. According to Fig. 4c, increasing the acidity from 9 to 4 increased the U(VI) ions removal efficiency. The experiments were repeated to investigate the effect of pH in the optimum condition (U(VI) concentration = 150 mg $L^{-1}$, NHAP concentration = 12.4 g $L^{-1}$, volume of ELM = 43 ml and retention time = 46 min); The results are compared with other reports in Table 3. Similar to other studies, the results showed that in acidic conditions the removal efficiency increases to 97.5%.

In this system, the immobilization of U(VI) ions may occur by three different mechanisms, includes surface adsorption, cation substitution, and dissolution-precipitation (Salman and Mohammed, 2019). According to the adsorption mechanism, the U(VI) ions are first adsorbed on the NHAP surface and then enter the ion exchange mechanism (Fig. 1). The ion exchange reaction can be expressed as the following stoichiometry:

$$Ca_{10}(PO_4)_6(OH)_2 + H_2O + UO_2^{2+} \rightarrow Ca(UO_2)_2(PO_4)_2(H_2O)_6 \quad (2)$$

Due to optimum pH, the main mechanism is dissolution-precipitation. At pH 4 the solubility of hydroxyapatite increases in the aqueous phase, the position of calcium ions in hydroxyapatite is replaced by U(VI) and precipitation occurs.

### 3.3.3. The volume ratio of emulsion to external phase

Emulsion to external for phase section in ELM processes affects the mass transfer, directly (Zereshki et al., 2018). Also, increasing emulsion phase increases removal efficiency but must consider globules stability conditions and operating costs (Razo-Lazcano et al., 2018). According to Fig. 4d with increasing the oil: wastewater ratio from 10:600 ml to about 45:600 ml, removal efficiency of U(VI) ions increased; but at 60:600 ml, removal efficiency decreased because the fluid mixing was not complete. Increasing the oil phase more than the optimum value in this process causes the emulsion globules to bind to each other and disrupt the filtration process with incomplete mixing. Lowering this ratio also reduces the efficiency of the filtration process (Salman and Mohammed, 2019), of course, the oil phase deficiency can be compensated by increasing the retention time and expanding the mixing in the system, somewhat.

### 3.3.4. The effect of retention time

Designing the proper geometry for the reactor stirring system, optimizing the material composition and temperature are affecting the retention time in the ELM process. Increasing retention time causes the emulsion globule to collide more with the impeller and the solar reactor wall which leads to break down large droplets, in other words, by shrinking the emulsion globules increase the contact surface (Kumar et al., 2019b). The results at ambient temperature (28 °C) showed that removal efficiency increased with rising retention time. According to Fig. 4e the removal efficiency of U(VI)ions increased rapidly after 5 min to about 50 min and decreased after 50–60 min, the reason is that after the optimal time, the temperature rises and the phenomenon of desorption occurs also, NHAP active sites are occupied.

According to ramps for the numerical optimization (Fig. 4f) and the experiment results, the optimum condition was selected as pH = 4, NHAP concentration = 12.4 g $L^{-1}$, volume of ELM = 43 ml and retention time = 45 min. In this study, by adjusting the conditions in the optimal state, the stability of the emulsion globules was obtained, however, by controlling the turbidity of the aqueous phase, it was ensured that apatite is not transferred from the oil phase to the aqueous phase.

### 3.4. Modeling of adsorption isotherms and thermodynamic parameters

The U(VI) ions in the wastewater, the ions pass through the oil layer and enter the ELM, the adsorption of U(VI) takes place on active sites of NHAP. To investigate the adsorption isotherm models, the adsorption process was performed at various concentrations (23, 144, 263, 379 and 499 mg $L^{-1}$) with optimum operating values (pH = 4, NHAP concentration = 12.4 g $L^{-1}$, volume of ELM = 43 ml and retention time = 45 min). The equilibrium concentration between heavy metal ions and adsorbent was investigated using adsorption isotherm equations. Eqs. (2), (3) and (4) represent the Langmuir, Freundlich, and Dubinin–Radushkevich isotherm, respectively.

$$\frac{C_e}{q_e} = \frac{1}{bq_{max}} + \frac{C_e}{q_{max}} \quad (3)$$

$$\log\frac{C_e}{q_e} = (1 - \frac{1}{n})\log C_e - \log q_{max} \quad (4)$$

$$\ln(q_e) = \ln(q_{max}) - \beta_{DR}\varepsilon^2 \quad (5)$$

where $q_e$ (mg $g^{-1}$) is the equilibrium U(VI) uptake capacity, $C_e$ (mg $L^{-1}$) is the equilibrium U(VI) ions concentration, $q_{max}$ is the highest mass of the U(VI) ions (unit gram) of

**Table 3** Comparison of pH and removal efficiency of heavy metals.

| Ion | Concentration ($mgL^{-1}$) | pH | Removal efficiency (%) | Reference |
|---|---|---|---|---|
| U(VI) | 150 | 10 | 32.2 | In this work |
| U(VI) | 150 | 9 | 60.1 | |
| U(VI) | 150 | 8 | 83.1 | |
| U(VI) | 150 | 6 | 93.7 | |
| U(VI) | 150 | 4 | 97.5 | |
| Cd (II) | 500 | 7.6 | 97 | (Benderrag et al., 2019) |
| U(VI) | 500 | 3 | 85 | (Kulkarni et al., 2002) |
| Cr(VI) | 100 | 0.45 | 97 | (Kumar et al., 2019b) |
| U(VI) | 300 | 4–4.5 | 99.5 | (Kulkarni et al., 2018) |
| Gd(III) | 50 | 2 | 99 | (Davoodi-Nasab et al., 2018) |
| Gd(III) | 50 | 1.56 | 67.45 | (Cui and Anderson, 2017) |
| Pb(II) | 200 | 3 | 97.2 | (Salman and Mohammed, 2019) |

NHAP. In the Eq. (2) b (L $mg^{-1}$) is the Langmuir amount with binding sites (Beni and Esmaeili, 2019a). n is the Freundlich constant in the Eq. (3) and related to intensity of the sorbent (Esmaeili and Beni, 2014). $\beta_{DR}$ ($mol^2$ $J^2$) is the activity coefficient in the Eq. (4);

$$\varepsilon = RTLn(1 + \frac{1}{C_e}) \quad (6)$$

The mean adsorption energy E; (kJ $mol^{-1}$) is as follows:

$$E = \left[\frac{1}{\sqrt{-2\beta_{DR}}}\right] \quad (7)$$

According to Table 4, the equilibrium data are agreement with the Langmuir isotherm model ($R^2$ >0.99) ie, adsorption occurs is favorable in the NHAP monolayer. As shown Dubinin–Radushkevich isotherm, energy of adsorption was <8 KJ $mol^{-1}$ so adsorption is adsorption for physical section. Analyses of isotherms for adsorption section showed the maximum amount of the U(VI)ions adsorption capacity ($q_{max}$) increased with increasing temperature. Also, according to Table 5 positive enthalpy ($\Delta H^{\circ}$) proves the interaction of ions and NHAP active sites is endothermic. The negative change in free energy ($\Delta G^{\circ}$) indicates feasibility and spontaneity of U (VI)ions adsorption.

### 3.5. Investigating the effect of sunlight and darkness control

The solar radiation technique was performed due to the use of solar energy to increase temperature, reducing viscosity and subsequently increasing the efficiency of absorption. For evaluate the solar radiation on the ELM performance, the removal efficiency of U(VI)ions at different retention times was calculated and fluid temperature inside the solar reactor was recorded. The condition in this experiment were as: pH = 4, NHAP dosage and ELM volume were optimized in 12.4 g $L^{-1}$ and 43 ml, respectively at highest initial concentration of U(VI)ions (500 mg $L^{-1}$).

As shown in Fig. 5a the ELM performance in the dark chamber had a removal efficiency of 68.53% after 60 min but, according to Fig. 5b the temperature of fluid increased from 28 °C to 45 °C after 60 min, so the adsorption process in this ELM was the endothermic nature. Also, U(VI) removal efficiency after 5 min at 28 °C was 10.28% but, increased to 92.3% at 60 min. The adsorption data of U(VI) ions at different retention times were analyzed by kinetic equations. According to Table 5, with pseudo first-order model fitted for U(VI) adsorption ($R^2$ >0.88). The adsorption process of U(VI) onto NHAP in the ELM was completed, after 60 min and then, to separate the oil and water phases, the system was idle for 45 min in stationary phase.

**Table 4** Isotherm parameters for U(VI) ions adsorption by ELM.

| T (K) | Experimental data | | Langmuir isotherm | | | Freundlich isotherm | | | Dubinin–Radushkevich isotherm | | | |
|---|---|---|---|---|---|---|---|---|---|---|---|---|
| | $C_e(mgL^{-1})$ | $q_e(mgg^{-1})$ | b $(Lmg^{-1})$ | $q_{max}$ $(mgg^{-1})$ | $R^2$ | n | $q_{max}$ $(mgg^{-1})$ | $R^2$ | $q_{max}$ $(mmolg^{-1})$ | $\beta_{DR}$ $(mol^2J^{-2})$ | E $(KJmol^{-1})$ | $R^2$ |
| 288 | 202 | 305 | 0.02 | 385 | 0.99 | 1.5 | 11.2 | 0.84 | 10.4 | $3 \times 10^{-6}$ | 0.41 | 0.92 |
| 301 | 118 | 301 | 0.02 | 526 | 0.99 | 1.4 | 16.5 | 0.80 | 11.2 | $1 \times 10^{-6}$ | 0.71 | 0.90 |
| 308 | 109 | 400 | 0.03 | 526 | 0.99 | 1.45 | 20 | 0.84 | 11.3 | $6 \times 10^{-7}$ | 0.91 | 0.90 |
| 313 | 97.9 | 412 | 0.03 | 526 | 0.99 | 1.42 | 21.6 | 0.79 | 11.4 | $6 \times 10^{-7}$ | 0.91 | 0.90 |
| 318 | 82.7 | 427 | 0.04 | 556 | 0.97 | 1.38 | 24.6 | 0.67 | 11.6 | $5 \times 10^{-7}$ | 1 | 0.90 |

**Table 5** Thermodynamic parameters for U(VI) ions adsorption by ELM. Summary of U(VI) sorption data evaluated by different kinetic models.

| Thermodynamic parameters | | | | | | | | | | | | |
|---|---|---|---|---|---|---|---|---|---|---|---|---|
| Concentration (mg $L^{-1}$) | $k_d$ | | | | | $\Delta H^{\circ}$ (kJ $mol^{-1}$) | $\Delta S^{\circ}$ (J $mol^{-1}$ $K^{-1}$) | $\Delta G^{\circ}$ (KJ $mol^{-1}$) | | | | |
| | 15 °C | 28 °C | 35 °C | 40 °C | 45 °C | | | 15 °C | 28 °C | 35 °C | 40 °C | 45 °C |
| 22.8 | 5.98 | 11.1 | 14 | 15 | 16.7 | 30.4 | 106 | −4.28 | −6.03 | −6.77 | −7.05 | −7.45 |
| 144 | 5.20 | 9.81 | 12.1 | 15 | 20.1 | 33.1 | 128 | −3.95 | −5.71 | −6.38 | −7.05 | −7.93 |
| 263 | 3.30 | 7.55 | 8.40 | 9.49 | 11.7 | 30.4 | 116 | −2.86 | −5.05 | −5.45 | −5.86 | −5.50 |
| 379 | 2.14 | 5.10 | 5.56 | 6.84 | 11.1 | 38.1 | 139 | −1.82 | −4.08 | −4.39 | −5.00 | −6.36 |
| 499 | 1.47 | 3.23 | 3.57 | 4.09 | 5.03 | 29.6 | 107 | −0.93 | −2.93 | −3.26 | −3.67 | −4.27 |

| Kinetic models | | | | | | | |
|---|---|---|---|---|---|---|---|
| Sample conditions | $q_{max}$ ($mgg^{-1}$) | First-order model | | | Second-order model | | |
| | | $k_1$ ($min^{-1}$) | $q_e$ (mg $g^{-1}$) | $R^2$ | $k_2$ (mg(g min)$^{-1}$) | $q_e$ (mg $g^{-1}$) | $R^2$ |
| In the dark room | 27 | 0.06 | 47.7 | 0.92 | $3 \times 10^{-3}$ | 127 | 0.79 |
| Under solar radiation | 36.3 | 0.05 | 58.4 | 0.88 | $2 \times 10^{-3}$ | 101 | 0.84 |

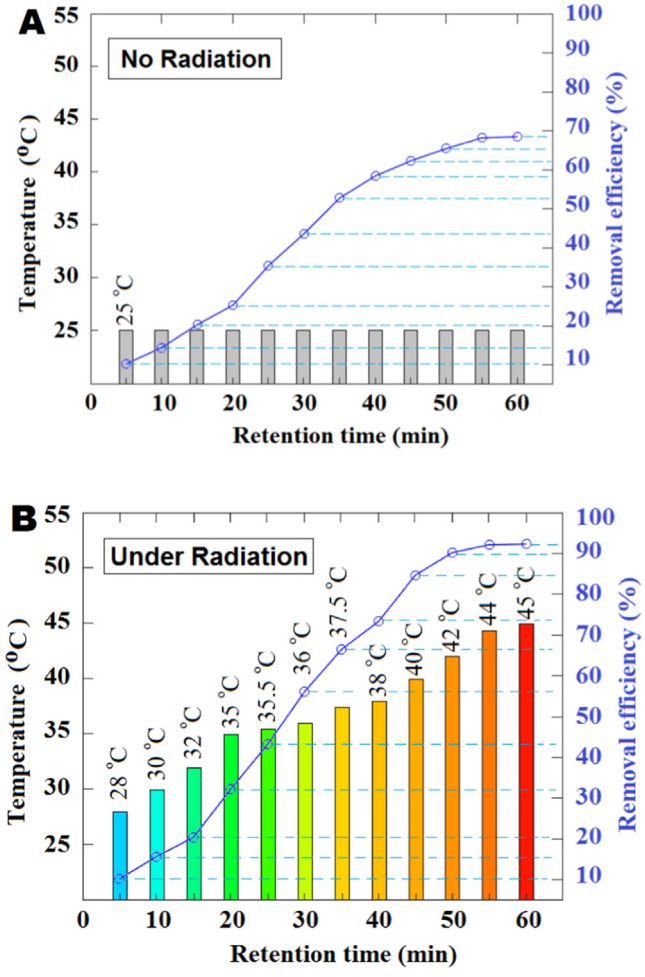


**Fig. 5** Effect of contact time on removal efficiency of U(VI) at the dark room (A) and the effect of solar radiation on the ELM performance (B).

## 4. Conclusions

The solar reactor based on NHAP in ELM system was used to remove U(VI) ions from the synthesized effluent. Entering the oil phase into the water phase with three needles equipped with vibrators using a syringe pump was a suitable technique for the formation of uniform emulsion globules. The parameters affecting the ELM process such as pH, NHAP concentration, volume of ELM, retention time, impeller rotational speed and air flow rate were optimized.

- The role of pH was important in dissolving U(VI) ions at fluid and transition from water phase to oil phase, so adjusting pH can increase removal efficiency.
- The U(VI) ions were adsorbed and immobilized on the NHAP surface in the oil phase.
- The aeration in solar reactor prevented the binding and growth of the emulsion globules; also aeration protected of globules from destruction by impeller rotation.
- CFD simulation showed the oil phase distribution in the water phase.
- Increasing the NHAP in oil phase more than optimum concentration, caused the emulsion globules to swell, NHAP were entered into water phase and increasing turbidity.
- The low rotational speed of the implant leads to the attachment and growth of the globules, and an increase in excess of the optimal amount causes the globules to break.
- The NHAP with about 50 nm of particle size in oil phase, were grouped after separations process.
- Solar radiation reduced the oil phase viscosity and made the process faster and more efficient.
- Based on the results, the techniques used in this work show that emulsion systems can be used on an industrial scale.

## Declaration of Competing Interest

The authors declare that they have no known competing financial interests or personal relationships that could have appeared to influence the work reported in this paper.

## Appendix A. Supplementary material

Supplementary data to this article can be found online at https://doi.org/10.1016/j.arabjc.2020.102959.

## References


Ahmad, A., Kusumastuti, A., Derek, C., Ooi, B., 2011. Emulsion liquid membrane for heavy metal removal: An overview on emulsion stabilization and destabilization. Chem. Eng. J. 171, 870–882.

Bayramoglu, G., Yakup Arica, M., 2016. MCM-41 silica particles grafted with polyacrylonitrile: Modification in to amidoxime and carboxyl groups for enhanced uranium removal from aqueous medium. Microporous Mesoporous Mater. 226, 117–124.

Bayramoglu, G., Yakup Arica, M., 2019. Star type polymer grafted and polyamidoximemodified silica coated-magnetic particles forad-sorption of U(VI) ions from solution. Chem. Eng. Res. Des. 147, 146–159.

Banat, F., Al-Bashir, B., Al-Asheh, S., Hayajneh, O., 2000. Adsorption of phenol by bentonite. Environ. Pollut. 107, 391–398.

Benderrag, A., Haddou, B., Daaou, M., Benkhedja, H., Bounaceur, B., Kameche, M., 2019. Experimental and modeling studies on Cd (II) ions extraction by emulsion liquid membrane using Triton X-100 as biodegradable surfactant. J. Environ. Chem. Eng. 7, 103166.

Beni, A.A., Esmaeili, A., 2019a. Biosorption, an efficient method for removing heavy metals from industrial effluents: A Review. Environ. Technol. Innov.

Beni, A.A., Esmaeili, A., 2019b. Design and optimization of a new reactor based on biofilm-ceramic for industrial wastewater treatment. Environ. Pollut. 255, 113298.

Christou, C., Philippou, K., Krasia-Christoforou, T., Pashalidis, I., 2019. Uranium adsorption by polyvinylpyrrolidone/chitosan blended nanofibers. Carbohydr. Polym. 219, 298–305.

Cui, H., Anderson, C.G., 2017. Alternative flowsheet for rare earth beneficiation of Bear Lodge ore. Miner. Eng. 110, 166–178.

Davoodi-Nasab, P., Rahabr-Kelishami, A., Safdari, J., 2019. Simultaneous effect of nanoparticles and surfactant on emulsion liquid membrane: Swelling, breakage and mean drop size. Sep. Purif. Technol. 219, 150–158.

Davoodi-Nasab, P., Rahbar-Kelishami, A., Safdari, J., Abolghasemi, H., 2017. Application of emulsion nanofluids membrane for the extraction of gadolinium using response surface methodology. J. Mol. Liq. 244, 368–373.

Davoodi-Nasab, P., Rahbar-Kelishami, A., Safdari, J., Abolghasemi, H., 2018. Evaluation of the emulsion liquid membrane performance on the removal of gadolinium from acidic solutions. J. Mol. Liq. 262, 97–103.

El Haddad, M., Slimani, R., Mamouni, R., Laamari, M.R., Rafqah, S., Lazar, S., 2013. Evaluation of potential capability of calcined bones on the biosorption removal efficiency of safranin as cationic dye from aqueous solutions. J. Taiwan Inst. Chem. Eng. 44, 13–18.

Esmaeili, A., Beni, A.A., 2014. A novel fixed-bed reactor design incorporating an electrospun PVA/chitosan nanofiber membrane. J. Hazard Mater. 280, 788–796.

Esmaeili, A., Beni, A.A., 2015. Novel membrane reactor design for heavy-metal removal by alginate nanoparticles. J. Ind. Eng. Chem. 26, 122–128.

Ferreira, L.C., Ferreira, L.C., Cardoso, V.L., Coutinho Filho, U., 2019. Mn (II) removal from water using emulsion liquid membrane composed of chelating agents and biosurfactant produced in loco. J. Water Process Eng. 29, 100792.

Guo, H., Jiang, C., Xu, Z., Luo, P., Fu, Z., Zhang, J., 2019. Synthesis of bitter gourd-shaped nanoscaled hydroxyapatite and its adsorption property for heavy metal ions. Mater. Lett. 241, 176–179.

Googerdchian, F., Moheb, A., Emadi, R., Asgari, M., 2018. Optimization of Pb(II) ions adsorption on nanohydroxyapatite adsorbents by applying Taguchi method. J. Hazard. Mater. 349, 186–194.

Han, M., Kong, L., Hu, X., Chen, D., Xiong, X., Zhang, H., Su, M., Diao, Z., Ruan, Y., 2018. Phase migration and transformation of uranium in mineralized immobilization by wasted bio-hydroxyapatite. J. Cleaner Prod. 197, 886–894.

Holmes, L.A., Turner, A., Thompson, R.C., 2012. Adsorption of trace metals to plastic resin pellets in the marine environment. Environ. Pollut. 160, 42–48.

Hubadillah, S.K., Othman, M.H.D., Tai, Z.S., Jamalludin, M.R., Yusuf, N.K., Ahmad, A., Rahman, M.A., Jaafar, J., Kadir, S.H.S. A., Harun, Z., 2020. Novel hydroxyapatite-based bio-ceramic hollow fiber membrane derived from waste cow bone for textile wastewater treatment. Chem. Eng. J. 379, 122396.

Jain, R., Peräniemi, S., Jordan, N., Vogel, M., Weiss, S., Foerstendorf, H., Lakaniemi, A.-M., 2018. Removal and recovery of uranium (VI) by waste digested activated sludge in fed-batch stirred tank reactor. Water Res. 142, 167–175.

Kohli, H.P., Gupta, S., Chakraborty, M., 2019. Stability and performance study of emulsion nanofluid membrane: A combined approach of adsorption and extraction of Ethylparaben. Colloids Surf., A 579, 123675.

Kulkarni, P., Mukhopadhyay, S., Bellary, M., Ghosh, S., 2002. Studies on membrane stability and recovery of uranium (VI) from aqueous solutions using a liquid emulsion membrane process. Hydrometallurgy 64, 49–58.

Kulkarni, S.S., Juvekar, V.A., Mukhopadhyay, S., 2018. Intensification of emulsion liquid membrane extraction of uranium (VI) by replacing nitric acid with sodium nitrate solution. Chem. Eng. Process.-Process Intensification 125, 18–26.

Kumar, A., Thakur, A., Panesar, P.S., 2019a. Recent developments on sustainable solvents for emulsion liquid membrane processes. J. Cleaner Prod. 118250.

Kumar, A., Thakur, A., Panesar, P.S., 2019b. A review on emulsion liquid membrane (ELM) for the treatment of various industrial effluent streams. Rev. Environ. Sci. Bio/Technol. 18, 153–182.

Long, Y., Jiang, J., Hu, J., Hu, X., Yang, Q., Zhou, S., 2019. Removal of Pb (II) from aqueous solution by hydroxyapatite/carbon composite: Preparation and adsorption behavior. Colloids Surf., A 577, 471–479.

Mesli, M., Belkhouche, N.-E., 2018. Extraction and pre-concentration of lead from copper by emulsion liquid membrane technique using an ionic liquid. Euro-Mediterranean J. Environ. Integration 3, 14.

Noah, N.F.M., Sulaiman, R.N.R., Othman, N., Jusoh, N., Rosly, M. B., 2020. Extractive continuous extractor for chromium recovery: Chromium (VI) reduction to chromium (III) in sustainable emulsion liquid membrane process. J. Cleaner Prod. 247, 119167.

Parbat, S.A., Bhanvase, B.A., Sonawane, S.H., 2020. Investigation on liquid emulsion membrane (LEM) prepared with hydrodynamic cavitation process for cobalt (II) extraction from wastewater. Sep. Purif. Technol. 237, 116385.

Piccirillo, C., Pereira, S., Marques, A.P., Pullar, R., Tobaldi, D., Pintado, M.E., Castro, P.M., 2013. Bacteria immobilisation on hydroxyapatite surface for heavy metals removal. J. Environ. Manage. 121, 87–95.

Razo-Lazcano, T.A., del Pilar González-Muñoz, M., Stambouli, M., Pareau, D., Hernández-Perales, L., Avila-Rodriguez, M., 2018. Chlorpheniramine recovery from aqueous solutions by emulsion

liquid membranes using soy lecithin as carrier. Colloids Surf., A 536, 68–73.
Sahu, M., Sar, S.K., Baghel, T., Dewangan, R., 2020. Seasonal and geochemical variation of uranium and major ions in groundwater at Kanker district of Chhattisgarh, central India. Groundwater Sustain. Dev. 10, 100330.
Salman, H.M., Mohammed, A.A., 2019. Extraction of lead ions from aqueous solution by co-stabilization mechanisms of magnetic Fe2O3 particles and nonionic surfactants in emulsion liquid membrane. Colloids Surf., A 568, 301–310.
Shin, W., Oh, J., Choung, S., Cho, B.-W., Lee, K.-S., Yun, U., Woo, N.-C., Kim, H.K., 2016. Distribution and potential health risk of groundwater uranium in Korea. Chemosphere 163, 108–115.
Sundaram, C.S., Viswanathan, N., Meenakshi, S., 2009. Fluoride sorption by nano-hydroxyapatite/chitin composite. J. Hazard. Mater. 172, 147–151.
Wu, Y., Chen, D., Kong, L., Tsang, D.C., Su, M., 2019. Rapid and effective removal of uranium (VI) from aqueous solution by facile synthesized hierarchical hollow hydroxyapatite microspheres. J. Hazard. Mater. 371, 397–405.
Zereshki, S., Daraei, P., Shokri, A., 2018. Application of edible paraffin oil for cationic dye removal from water using emulsion liquid membrane. J. Hazard. Mater. 356, 1–8.
Zhao, X.-Y., Zhu, Y.-J., Zhao, J., Lu, B.-Q., Chen, F., Qi, C., Wu, J., 2014. Hydroxyapatite nanosheet-assembled microspheres: Hemoglobin-templated synthesis and adsorption for heavy metal ions. J. Colloid Interface Sci. 416, 11–18.
Yakup Arica, M., Bayramoglu, G., 2016. Polyaniline coated magnetic carboxymethylcellulose beads for selective removal of uranium ions from aqueous solution. J. Radioanal. Nucl. Chem. 310, 711–724.